Magnetic response of Sr_2RuO_4: quasi-local spin fluctuations due to Hund's coupling

Hugo U. R. Strand,[1, *] Manuel Zingl,[1] Nils Wentzell,[1] Olivier Parcollet,[1, 2] and Antoine Georges[1, 3, 4, 5]

[1]*Center for Computational Quantum Physics, Flatiron institute,*
Simons Foundation, 162 5th Ave., New York, 10010 NY, USA
[2]*Institut de Physique Théorique (IPhT), CEA, CNRS, UMR 3681, 91191 Gif-sur-Yvette, France*
[3]*Collège de France, 11 place Marcelin Berthelot, 75005 Paris, France*
[4]*Centre de Physique Théorique, Ecole Polytechnique, CNRS, 91128 Palaiseau Cedex, France*
[5]*Department of Quantum Matter Physics, University of Geneva,*
24 Quai Ernest-Ansermet, 1211 Geneva 4, Switzerland
(Dated: April 17, 2019)

We study the magnetic susceptibility in the normal state of Sr_2RuO_4 using dynamical mean-field theory including dynamical vertex corrections. Besides the well known incommensurate response, our calculations yield quasi-local spin fluctuations which are broad in momentum and centered around the Γ point, in agreement with recent inelastic neutron scattering experiments [P. Steffens, *et al.*, Phys. Rev. Lett. **122**, 047004 (2019)]. We show that these quasi-local fluctuations are controlled by the Hund's coupling and account for the dominant contribution to the momentum-integrated response. While all orbitals contribute equally to the incommensurate response, the enhanced Γ point response originates from the planar xy orbital.

The importance of spin fluctuations for the physics of Sr_2RuO_4 has been emphasized long ago [1]. This material is close to a spin-density-wave instability and small concentrations of impurities trigger ordering [2, 3]. Inelastic neutron scattering experiments (INS) pioneered by Sidis *et al.* [1] and refined over the years [4–10] have revealed that the magnetic response is essentially the sum of (i) a weakly momentum-dependent contribution centered at Γ (in agreement with the Stoner enhancement factor of the uniform susceptibility by ~ 7 as compared to the band value [11, 12]) and (ii) a peak at an incommensurate wavevector $\mathbf{Q}_{SDW} \approx (0.3, 0.3, 0)$ [13] signaling the proximity to a spin-density-wave (SDW) instability [10]. The peak at $\mathbf{Q}_{SDW}$ was predicted by Mazin and Singh [14] using density functional theory (DFT) and the random phase approximation (RPA). However, DFT+RPA does not account for the broad structure at Γ, and it also predicts substantial anti-ferromagnetic fluctuations at the X point, $\mathbf{Q}_X = (0.5, 0.5, 0)$, in contradiction to experiments [10].

More recently, however, it has been realized that the origin of the strong correlations in this material may not be associated with long-wavelength magnetic correlations, but with local correlations driven by the Hund's coupling [15, 16]. A successful description of an extensive set of physical properties of Sr_2RuO_4 has been obtained following this picture, supported by quantitative dynamical mean-field (DMFT) calculations. This includes the large mass enhancements of quasiparticles observed in de Haas-van Alphen experiments [17] and angle resolved photo-emission spectroscopy [18], as well as quasi-particle weights and lifetimes [15], nuclear magnetic resonance [15], optical conductivity [19, 20], thermopower [21], Hall coefficient [22], quasiparticle dispersions [23–25], and magnetic response [26–29].

In this letter, we bridge this gap between the spin fluc-tuations picture and the Hund's metal picture of the normal state of Sr_2RuO_4 by analyzing the magnetic response function using DMFT. Our results reproduce the overall momentum dependence obtained in experiments [10], see Fig. 1, and reveal strong coupling effects which cannot be accounted for in RPA, such as a suppression of the antiferromagnetic response at $\mathbf{Q}_X$. We find that the response is dominated by quasi-local (weakly momentum-dependent) spin fluctuations, and show that these fluctuations are controlled by the strength of the Hund's coupling. As discussed at the end of this letter, our findings have direct relevance for theories of the superconducting pairing mechanism, which is still an outstanding and much debated question [30].

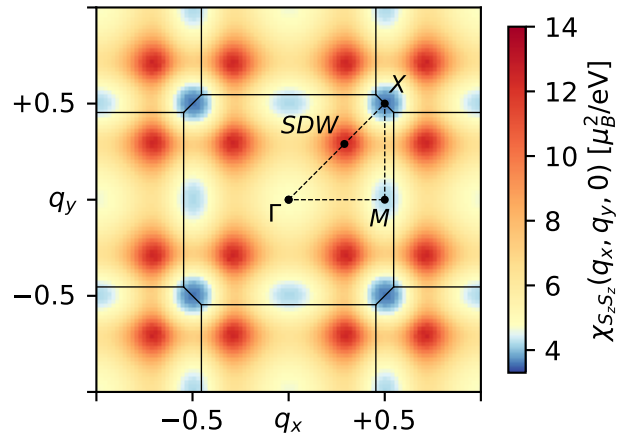We compute the magnetic susceptibility $\chi_{S_z S_z}(\mathbf{Q})$ us-

FIG. 1. Spin-susceptibility $\chi_{S_z S_z}(\mathbf{Q})$ from DMFT at $T = 464\,\mathrm{K}$ in the q_x, q_y-plane at $q_z = 0$, with incommensurate hot-spots at $\mathbf{Q}_{SDW}$ (red), cold-spots at $\mathbf{Q}_M$ and $\mathbf{Q}_X$ (blue), and a broad response centered around $\mathbf{Q}_\Gamma$ (yellow), in units of the reciprocal tetragonal lattice vectors $2\pi/a$ and $2\pi/c$.

ing DMFT [31], a DFT derived effective three-band t_{2g} model without spin-orbit coupling [32], and a local Kanamori interaction [33] with Hubbard $U = 2.3\,\text{eV}$ and Hund's $J = 0.4\,\text{eV}$ [15]. The DMFT equations were solved using the hybridization expansion continuous time quantum Monte Carlo [34] implementation in TRIQS [35, 36]. The DMFT particle-hole irreducible vertex was used to compute the static lattice susceptibility from the Bethe-Salpeter equation (BSE) [31] as implemented in the TRIQS two-particle response function toolbox [37]. Moreover, the static response at three specific momenta was computed down to much lower temperature, using self-consistent DMFT in applied magnetic fields by zero field extrapolation in supercells.

Fig. 1 displays the momentum dependent magnetic susceptibility from DMFT, with hot-spots at $\mathbf{Q}_{SDW}$ and ridges in q_x and q_y connecting these hot spots. This SDW component can be understood from the DFT electronic structure [38] of this material, which has three Ru(4d)-t_{2g} bands crossing the Fermi level, filled with four electrons. The quasi-two-dimensional γ band, with dominant xy orbital content, has a larger bandwidth (by a factor of ~ 2) and slightly lower energy than the quasi-one-dimensional α and β bands, originating mainly from the xz and yz orbitals. The peak at $\mathbf{Q}_{SDW}$ is generated by nesting in the α and β (xz, yz) Fermi surface sheets, yielding ridges at $(0.3, q_y, 0)$ and $(q_x, 0.3, 0)$ that cross and produce the peak at $\mathbf{Q}_{SDW}$ [14].

The response in Fig. 1 also shows a large component, broad in momentum, with enhanced intensity centered at Γ in comparison to the cold-spots at M and X. This is the signature of the important quasi-local spin fluctuations. Antiferromagnetic fluctuations are suppressed, with the X point being the global minimum of the response. This is qualitatively different from the results of weak-coupling approaches such as RPA [14, 39–42] – even when basing RPA on the dressed DMFT Lindhard function [28] – or the fluctuation-exchange approximation [43, 44]. In contrast, these approximations yield an enhanced response at the X point and fail to account for the quasi-local response. The latter was not discussed in previous DMFT work [27], but noted in a recent DMFT+GW calculation [29]. Both the quasi-local response and the suppression of the X-point fluctuations are in qualitative agreement with the recent INS experiments [10].

Studying the susceptibility along the high symmetry path Γ–X–M–Γ–Z gives a quantitative picture of the response, see Fig. 2a. The incommensurate response at $\mathbf{Q}_{SDW}$ yields a peak on Γ–X and the nesting ridges become local maxima on X–M and M–Γ. The response at $\mathbf{Q}_\Gamma = (0,0,0)$ is enhanced relative to the cold-spots at $\mathbf{Q}_X = (0.5, 0.5, 0)$ and $\mathbf{Q}_M = (0.5, 0, 0)$ (green-shaded area) with $\mathbf{Q}_X$ being the global minimum. We note in passing that the negligible dispersion on Γ–Z shows that the response is quasi two-dimensional. The quasi-local
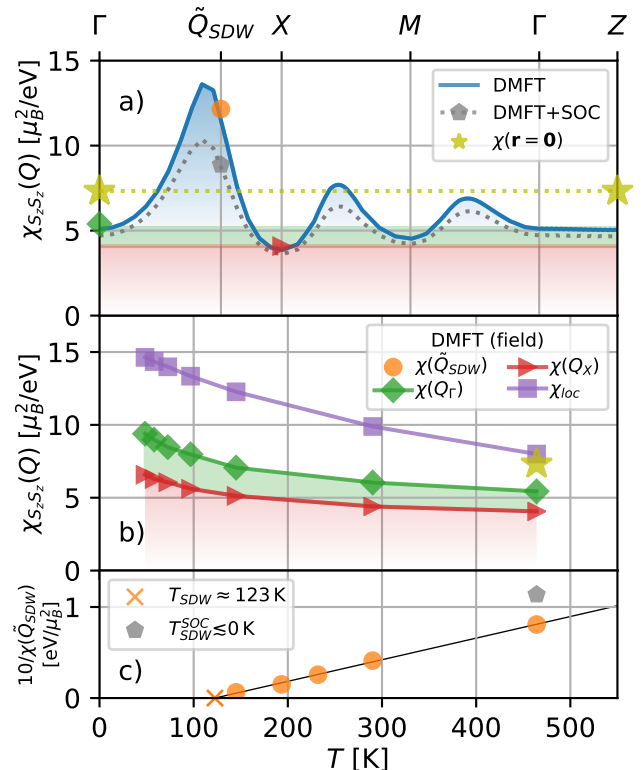

FIG. 2. a) Spin-susceptibility $\chi_{S_z S_z}(\mathbf{Q})$ from DMFT at $T = 464\,\text{K}$, along the high-symmetry path Γ–X–M–Γ–Z (see Fig. 1) with (gray dotted line) and without (blue line) SOC, together with the applied field response at $\mathbf{Q}_\Gamma$ (green diamond), $\mathbf{Q}_X$ (red triangle), $\tilde{\mathbf{Q}}_{SDW}$ (orange circle), and $\chi(\mathbf{r}=\mathbf{0})$ (yellow star). b) Temperature dependence of $\chi(\mathbf{Q}_X)$, $\chi(\mathbf{Q}_\Gamma)$, and χ_{loc}. c) Temperature dependence of $1/\chi(\tilde{\mathbf{Q}}_{SDW})$ without (circles) and with (pentagon) SOC.

response (red- and green-shaded area) is the dominant part of the susceptibility, accounting for more than half of the momentum averaged response (yellow stars).

We also perform complementary calculations of the susceptibility down to much lower temperature through self-consistent DMFT in applied fields at $\mathbf{Q}_\Gamma$, $\mathbf{Q}_X$, and in the vicinity of the incommensurate wave vector $\mathbf{Q}_{SDW}$ at $\tilde{\mathbf{Q}}_{SDW} = (1/3, 1/3, 0)$ (using a $\sqrt{2} \times \sqrt{5}$ three site supercell), see Fig. 2b and 2c. The result is in quantitative agreement with the DMFT response obtained from the BSE after extrapolating to infinite fermionic frequency cutoff [45], see markers in Fig. 2a. This serves as a nontrivial consistency check of our calculations and is, to the best of our knowledge, the first demonstration of thermodynamical consistency in DMFT at the two-particle level in a multiorbital model [31, 46, 47].

When lowering temperature the spin susceptibility is enhanced, see Fig. 2b. In particular, both $\chi(\mathbf{Q}_\Gamma)$ and $\chi(\mathbf{Q}_X)$ grow with decreasing temperature, where $\chi(\mathbf{Q}_X)$ can be taken as a direct measure of the background response (red shaded area). However, the relative Γ point enhancement (green shaded area) is robust and roughly

constant, $\chi(\mathbf{Q}_\Gamma)/\chi(\mathbf{Q}_X) \approx 4/3$, in the studied temperature range. The precise value of this ratio, however, strongly depends on J (see below). The DMFT local impurity susceptibility χ_{loc} shows a similar temperature dependence, and is approximately equal to the local susceptibility $\chi(\mathbf{r} = \mathbf{0}) \equiv \frac{1}{V} \sum_\mathbf{Q} \chi(\mathbf{Q})$ at $T = 464\,\mathrm{K}$. This rough agreement strengthens the use of χ_{loc} as a proxy for the momentum average, $\chi_{loc} \sim \chi(\mathbf{r} = \mathbf{0})$ [15, 21].

While it is known that pristine Sr_2RuO_4 does not order magnetically [12], the question of whether DMFT yields SDW order at low temperature (like DFT [48]) has not been addressed previously. To answer this question we make a linear extrapolation of $\chi^{-1}(\tilde{\mathbf{Q}}_{SDW})$ in temperature, see Fig. 2c. For the established values of U and J [15], and in the absence of spin-orbit coupling, we find that DMFT yields SDW order at $T_{SDW} \approx 123\,\mathrm{K}$, much lower than RPA [49]. However, the transition temperature is very sensitive to the precise value of the microscopic parameters, in particular the Hund's coupling J (not shown).

The sensitivity in J raises the question how the relatively small spin-orbit coupling (SOC) $\lambda_{DFT} \approx 0.1\,\mathrm{eV}$ [23] affects the ordering temperature. Full DMFT calculations with SOC, in the relevant temperature range, are out of reach with currently available algorithms. Instead we resort to an approximate treatment – following Ref. 24 – and add a static self-energy correction to the DMFT bubble in the BSE, with a correlation-enhanced SOC coupling $\lambda = 2\lambda_{DFT}$, see also Ref. 50. This accounts for the first order SOC contributions to the DMFT bubble $\chi^{(0)}$ but neglects the effect of SOC on the vertex. In momentum space the magnetic susceptibility with SOC corrections exhibits an overall suppression of the incommensurate and ridge response while the Γ, X, and M points are only weakly affected, see Fig. 2a. The reduced incommensurate response yields a higher inverse susceptibility, see Fig. 2c, shifting the transition to lower temperature. Using the linear slope of the non-SOC case gives $T_{SDW}^{SOC} \lesssim 0$. Our tentative conclusion is thus that a full DMFT+SOC calculation down to low temperature is likely not to yield SDW ordering. This obviously deserves further studies. Since the inclusion of SOC primarily affects the SDW response, which is not the main focus of our study, we will neglect it in the following.

To disentangle the microscopic mechanisms driving the different components of the magnetic response, we study their dependence on the Hund's coupling J, see Fig. 3. While the incommensurate spin-density-wave response $\chi(\tilde{\mathbf{Q}}_{SDW})$ displays a non-monotonic behavior in J, increasing J suppresses $\chi(\mathbf{Q}_X)$ and drastically increases $\chi(\mathbf{Q}_\Gamma)$ and χ_{loc}. Hence, the Hund's coupling drives the observed Γ point enhancement (green shaded area in Figs. 2a and 2b), as well as the enhancement of the local susceptibility. Since the response around the Γ point is very broad in momentum space (see Fig. 1) this in turn suggests that the Hund's coupling is responsible for the
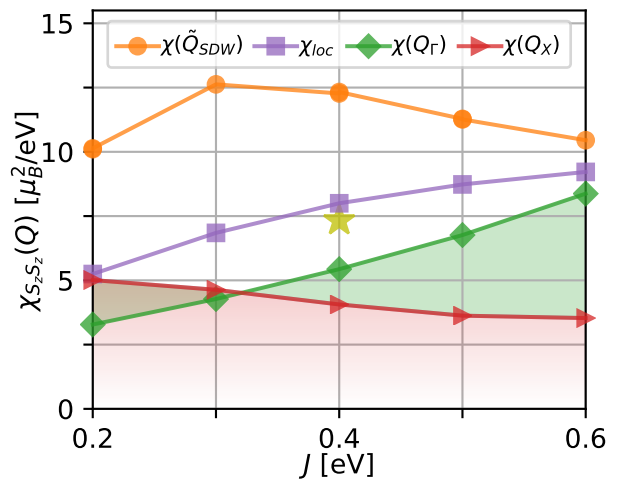

FIG. 3. Spin-susceptibility $\chi_{S_zS_z}(\mathbf{Q})$ for $T = 464\,\mathrm{K}$ from DMFT at $\tilde{\mathbf{Q}}_{SDW}$ (orange circles), $\mathbf{Q}_\Gamma$ (green diamonds), $\mathbf{Q}_X$ (red triangles), and the impurity local susceptibility χ_{loc} (purple squares), as a function of J at $U = 2.3\,\mathrm{eV}$ and around $J = 0.4\,\mathrm{eV}$. The local lattice susceptibility $\chi(\mathbf{r}=\mathbf{0})$ (yellow star) is also shown.

overall quasi-local magnetic response. We note in passing that the opposite trends of $\chi(\mathbf{Q}_\Gamma)$ and $\chi(\mathbf{Q}_X)$ as a function of J produces a qualitative change of the magnetic response at $J \sim 0.32\,\mathrm{eV}$ where the two terms cross. We conclude that the Hund's coupling is responsible for the enhanced quasi-local fluctuations and plays a key role in the overall momentum space structure of the magnetic response.

We finally investigate how the magnetic response is distributed over the planar xy, and out-of-plane xz and yz orbitals, by studying the decomposition

$$\chi(\mathbf{Q}) \equiv \chi_{S_zS_z}(\mathbf{Q}) = \sum_{ab} \chi_{S_z^{(a)}S_z^{(b)}}(\mathbf{Q}), \quad a, b \in \{xy, xz, yz\},$$

shown in Fig. 4a. We find that the orbital-off-diagonal response ($a \neq b$) is roughly 50% of the total magnetic response and confirm [27] that xy, xz, and yz contribute approximately equally to the $\mathbf{Q}_{SDW}$ response, see markers in Fig. 4. However, $\chi_{S_z^{(xy)}S_z^{(xy)}}(\mathbf{Q})$ is markedly higher than $\chi_{S_z^{(xz)}S_z^{(xz)}}(\mathbf{Q})$ around Γ and along $M-\Gamma$. It is this part of the $\chi_{S_z^{(xy)}S_z^{(xy)}}(\mathbf{Q})$ response, shown in Fig. 4b, that is the origin of the broad plateau around Γ and cold spots at X and M in Fig. 1, and the $\mathbf{Q}_\Gamma$ enhancement (green area) in Fig. 2a. While this only gives a weak momentum dependence to the large quasi-local magnetic response (red and green areas in Fig. 2a), the momentum space variations are extremely sensitive to the Hund's coupling, as seen in Fig. 3.

We now compare our results to simpler approximations and show that the DMFT results are the only one qualitatively compatible with experiments and that the full frequency-dependent vertex is a crucial part of the cal-
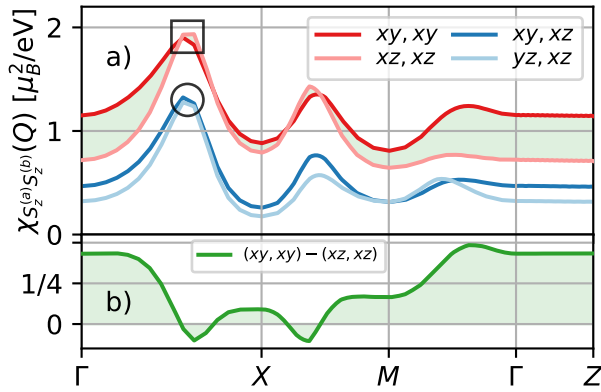
FIG. 4. a) Orbitally resolved $\chi_{S_z^{(a)} S_z^{(b)}}(\mathbf{Q})$ with $a, b \in \{xy, xz, yz\}$ at $T = 464\,\mathrm{K}$ from DMFT with diagonal xy, xy (red) and xz, xz (light red) response and off-diagonal xy, xz (blue) and yz, xz response (light blue) which contribute equally at $\mathbf{Q}_{SDW}$ (black markers). b) The difference in the diagonal orbital response $(xy, xy) - (xz, xz)$ (green).

FIG. 5. a) Spin-susceptibility $\chi_{S_z S_z}(\mathbf{Q})$ at $T = 464\,\mathrm{K}$ on the high-symmetry path $\Gamma-X-M-\Gamma-Z$ (see Fig. 1). The DMFT response (blue) is compared to the the screened RPA result (purple) and the DFT (green) and DMFT (orange) bare bubbles $\chi^{(0)}_{S_z S_z}(\mathbf{Q}) \propto GG$. Note the scaling of the dashed lines. Planar cuts at $q_z = 0$ for b) DFT and c) screened RPA are also shown, cf. DMFT in Fig. 1.

culation which can not be neglected [51]. Indeed, in Fig. 5a the DMFT result is compared to the bare DFT and DMFT bubbles ($\chi^{(0)}_{\mathrm{DFT}}$, $\chi^{(0)}_{\mathrm{DMFT}}$) and the screened RPA result χ_{RPA}. The RPA calculation uses – in spirit of Ref. 28 – the DMFT bubble $\chi^{(0)}$ and screened effective interaction parameters $\tilde{U} = 1.37\,\mathrm{eV}$ and $\tilde{J}/\tilde{U} = 0.4/2.3$, where $\tilde{U}$ has been taken to reproduce the local susceptibility $\chi(\mathbf{r} = \mathbf{0}) \approx 7.3\,\mu_B^2/\mathrm{eV}$ of DMFT. The frequency dependent particle-hole vertex is clearly essential in the DMFT calculation, as $\chi^{(0)}_{\mathrm{DMFT}}$ is much smaller than the DMFT result χ_{DMFT}. $\chi^{(0)}_{\mathrm{DFT}}$ is also strongly suppressed compared to χ_{DMFT}, and the X-point response is higher than both the Γ and M points (see Fig. 5b). Finally, the screened RPA using the DMFT bubble χ_{RPA} severely overestimates the strength of the nesting peaks, underestimates the constant background response, and fails both to enhance $\chi(\mathbf{Q}_\Gamma)$ and to suppress $\chi(\mathbf{Q}_X)$, see Fig. 5c.

In conclusion, we have analyzed the momentum-dependent magnetic response of $\mathrm{Sr_2RuO_4}$ using dynamical mean-field theory, taking full account of vertex corrections. The latter are found to play a crucial role, leading to key effects absent at the RPA level such as the suppression of the antiferromagnetic response at $\mathbf{Q}_X$. In agreement with neutron scattering experiments [10], the magnetic response has two main components: an SDW incommensurate response at $\mathbf{Q}_{SDW}$ and a quasi-local weakly momentum-dependent component, which provides the main contribution to the overall momentum integrated response. Our main result, on a qualitative level, is the demonstration that the physical origin of the quasi-local magnetic response is the Hund's coupling, hence reconciling the experimental emphasis put on spin fluctuations in this material with the theoretical picture of $\mathrm{Sr_2RuO_4}$ as a 'Hund's metal'.
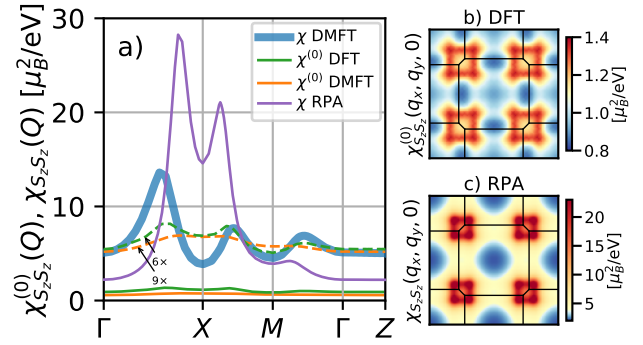
This has far-reaching consequences: both our theoreti-

cal calculations and neutron scattering experiments indicate that there is no dispersing 'quasi-ferromagnetic' spin fluctuation mode in $\mathrm{Sr_2RuO_4}$. Hence, pairing mechanisms based on a mediating bosonic mode ('glue') associated with ferromagnetic spin fluctuations [11, 12, 14, 52] have to be seriously reconsidered. The observed suppression of the magnetic response at the X point also invalidates an antiferromagnetic 'glue'. Instead, pairing mechanisms based on a quasi-local mode associated with Hund's coupling offer a promising route. Recent work has appeared in this direction for model Hamiltonians [53–55] and for iron-based superconductors [56]. However, these mechanisms were proposed in the regime of slow spin fluctuations above the Fermi liquid temperature, and need to be extended to be applicable to $\mathrm{Sr_2RuO_4}$. This is a key agenda for future work aiming at solving the 25-years old puzzle of superconductivity in this material [30].

* hugo.strand@gmail.com
[1] Y. Sidis, M. Braden, P. Bourges, B. Hennion, S. NishiZaki, Y. Maeno, and Y. Mori, Phys. Rev. Lett. **83**, 3320 (1999).
[2] M. Minakata and Y. Maeno, Phys. Rev. B **63**, 180504(R) (2001).

[3] M. Braden, O. Friedt, Y. Sidis, P. Bourges, M. Minakata, and Y. Maeno, Phys. Rev. Lett. **88**, 197002 (2002).

[4] F. Servant, B. Fåk, S. Raymond, J. P. Brison, P. Lejay, and J. Flouquet, Phys. Rev. B **65**, 184511 (2002).

[5] M. Braden, Y. Sidis, P. Bourges, P. Pfeuty, J. Kulda, Z. Mao, and Y. Maeno, Phys. Rev. B **66**, 064522 (2002).

[6] M. Braden, O. Friedt, Y. Sidis, P. Bourges, P. Pfeuty, S. Nakatsuji, Z. Mao, N. Kikugawa, M. Minakata, and Y. Maeno, Physica C **388**, 489 (2003).

[7] M. Braden, P. Steffens, Y. Sidis, J. Kulda, P. Bourges, S. Hayden, N. Kikugawa, and Y. Maeno, Phys. Rev. Lett. **92**, 097402 (2004).

[8] K. Iida, M. Kofu, N. Katayama, J. Lee, R. Kajimoto, Y. Inamura, M. Nakamura, M. Arai, Y. Yoshida, M. Fujita, K. Yamada, and S.-H. Lee, Phys. Rev. B **84**, 060402(R) (2011).

[9] K. Iida, J. Lee, M. B. Stone, M. Kofu, Y. Yoshida, and S. Lee, J. Phys. Soc. Jpn. **81**, 124710 (2012).

[10] P. Steffens, Y. Sidis, J. Kulda, Z. Q. Mao, Y. Maeno, I. I. Mazin, and M. Braden, Phys. Rev. Lett. **122**, 047004 (2019).

[11] T. M. Rice and M. Sigrist, J. Phys.: Condens. Matter **7**, L643 (1995).

[12] A. P. Mackenzie and Y. Maeno, Rev. Mod. Phys. **75**, 657 (2003).

[13] In units of the reciprocal tetragonal lattice vectors $2\pi/a$ and $2\pi/c$.

[14] I. I. Mazin and D. J. Singh, Phys. Rev. Lett. **82**, 4324 (1999).

[15] J. Mravlje, M. Aichhorn, T. Miyake, K. Haule, G. Kotliar, and A. Georges, Phys. Rev. Lett. **106**, 096401 (2011).

[16] A. Georges, L. d. Medici, and J. Mravlje, Ann. Rev. Cond. Mat. Phys. **4**, 137 (2013).

[17] A. P. Mackenzie, S. R. Julian, A. J. Diver, G. J. McMullan, M. P. Ray, G. G. Lonzarich, Y. Maeno, S. Nishizaki, and T. Fujita, Phys. Rev. Lett. **76**, 3786 (1996); C. Bergemann, S. R. Julian, A. P. Mackenzie, S. NishiZaki, and Y. Maeno, Phys. Rev. Lett. **84**, 2662 (2000); C. Bergemann, A. P. Mackenzie, S. R. Julian, D. Forsythe, and E. Ohmichi, Adv. Phys. **52**, 639 (2003).

[18] A. P. Mackenzie, S.-i. Ikeda, Y. Maeno, T. Fujita, S. R. Julian, and G. G. Lonzarich, J. Phys. Soc. Jpn. **67**, 385 (1998); A. Damascelli, D. H. Lu, K. M. Shen, N. P. Armitage, F. Ronning, D. L. Feng, C. Kim, Z.-X. Shen, T. Kimura, Y. Tokura, Z. Q. Mao, and Y. Maeno, Phys. Rev. Lett. **85**, 5194 (2000); H. Iwasawa, Y. Aiura, T. Saitoh, I. Hase, S. I. Ikeda, Y. Yoshida, H. Bando, M. Higashiguchi, Y. Miura, X. Y. Cui, K. Shimada, H. Namatame, and M. Taniguchi, Phys. Rev. B **72**, 104514 (2005); N. J. C. Ingle, K. M. Shen, F. Baumberger, W. Meevasana, D. H. Lu, Z.-X. Shen, A. Damascelli, S. Nakatsuji, Z. Q. Mao, Y. Maeno, T. Kimura, and Y. Tokura, Phys. Rev. B **72**, 205114 (2005); H. Iwasawa, Y. Yoshida, I. Hase, S. Koikegami, H. Hayashi, J. Jiang, K. Shimada, H. Namatame, M. Taniguchi, and Y. Aiura, Phys. Rev. Lett. **105**, 226406 (2010); H. Iwasawa, Y. Yoshida, I. Hase, K. Shimada, H. Namatame, M. Taniguchi, and Y. Aiura, Phys. Rev. Lett. **109**, 066404 (2012); V. B. Zabolotnyy, D. V. Evtushinsky, A. A. Kordyuk, T. K. Kim, E. Carleschi, B. P. Doyle, R. Fittipaldi, M. Cuoco, A. Vecchione, and S. V. Borisenko, J. Electron Spectros. Relat. Phenomena **191**, 48 (2013); B. Burganov, C. Adamo, A. Mulder,

M. Uchida, P. D. C. King, J. W. Harter, D. E. Shai, A. S. Gibbs, A. P. Mackenzie, R. Uecker, M. Bruetzam, M. R. Beasley, C. J. Fennie, D. G. Schlom, and K. M. Shen, Phys. Rev. Lett. **116**, 197003 (2016).

[19] D. Stricker, J. Mravlje, C. Berthod, R. Fittipaldi, A. Vecchione, A. Georges, and D. van der Marel, Phys. Rev. Lett. **113**, 087404 (2014).

[20] X. Deng, K. Haule, and G. Kotliar, Phys. Rev. Lett. **116**, 256401 (2016).

[21] J. Mravlje and A. Georges, Phys. Rev. Lett. **117**, 036401 (2016).

[22] M. Zingl, J. Mravlje, M. Aichhorn, O. Parcollet, and A. Georges, arXiv:1902.05503 (2019).

[23] G. Zhang, E. Gorelov, E. Sarvestani, and E. Pavarini, Phys. Rev. Lett. **116**, 106402 (2016).

[24] M. Kim, J. Mravlje, M. Ferrero, O. Parcollet, and A. Georges, Phys. Rev. Lett. **120**, 126401 (2018).

[25] A. Tamai, M. Zingl, E. Rozbicki, E. Cappelli, S. Ricco, A. de la Torre, S. McKeown Walker, F. Y. Bruno, P. D. C. King, W. Meevasana, M. Shi, M. Radovic, N. C. Plumb, A. S. Gibbs, A. P. Mackenzie, C. Berthod, H. Strand, M. Kim, A. Georges, and F. Baumberger, arXiv:1812.06531 (2018).

[26] L. V. Boehnke, *Susceptibilities in materials with multiple strongly correlated orbitals*, Ph.D. thesis, Universität Hamburg (2014).

[27] L. Boehnke, P. Werner, and F. Lechermann, EPL **122**, 57001 (2018).

[28] O. Gingras, R. Nourafkan, A.-M. S. Tremblay, and M. Côté, arXiv:1808.02527 (2018).

[29] S. Acharya, D. Pashov, C. Weber, H. Park, L. Sponza, and M. van Schilfgaarde, arXiv:1811.05143 (2018).

[30] A. P. Mackenzie, T. Scaffidi, C. W. Hicks, and Y. Maeno, npj Quantum Mat. **2**, 40 (2017).

[31] A. Georges, G. Kotliar, W. Krauth, and M. J. Rozenberg, Rev. Mod. Phys. **68**, 13 (1996).

[32] The model is identical to the one used in [25] and derived from a density functional theory (DFT) calculation of Sr_2RuO_4 in the experimental structure [57] (at 100 K) using Wien2k [58] with PBE [59] and 20^3 k-points. Maximally-localized t_{2g} Wannier functions were constructed using wien2wannier [60] and Wannier90 [61–63] (using 10^3 k-points).

[33] J. Kanamori, Prog. Theor. Phys. **30**, 275 (1963).

[34] P. Werner, A. Comanac, L. de' Medici, M. Troyer, and A. J. Millis, Phys. Rev. Lett. **97**, 076405 (2006); P. Werner and A. J. Millis, Phys. Rev. B **74**, 155107 (2006); K. Haule, Phys. Rev. B **75**, 155113 (2007); E. Gull, A. J. Millis, A. I. Lichtenstein, A. N. Rubtsov, M. Troyer, and P. Werner, Rev. Mod. Phys. **83**, 349 (2011).

[35] O. Parcollet, M. Ferrero, T. Ayral, H. Hafermann, I. Krivenko, L. Messio, and P. Seth, Comput. Phys. Commun. **196**, 398 (2015).

[36] P. Seth, I. Krivenko, M. Ferrero, and O. Parcollet, Comput. Phys. Commun. **200**, 274 (2016).

[37] H. U. R. Strand, github.com/TRIQS/tprf (2019), doi:10.5281/zenodo.2638059.

[38] T. Oguchi, Phys. Rev. B **51**, 1385 (1995); D. J. Singh, Phys. Rev. B **52**, 1358 (1995); I. Hase and Y. Nishihara, J. Phys. Soc. Jpn. **65**, 3957 (1996); G. J. McMullan, M. P. Ray, and R. J. Needs, Physica B: Cond. Mat. **223-224**, 529 (1996); P. K. de Boer and R. A. de Groot, Phys. Rev. B **59**, 9894 (1999); E. Pavarini and I. I. Mazin,

Phys. Rev. B **74**, 035115 (2006).

[39] D. K. Morr, P. F. Trautman, and M. J. Graf, Phys. Rev. Lett. **86**, 5978 (2001).

[40] K.-K. Ng and M. Sigrist, J. Phys. Soc. Jpn. **69**, 3764 (2000).

[41] I. Eremin, D. Manske, and K. H. Bennemann, Phys. Rev. B **65**, 220502(R) (2002).

[42] I. Eremin, D. Manske, C. Joas, and K. H. Bennemann, EPL **58**, 871 (2002).

[43] N. Arakawa, Phys. Rev. B **90**, 245103 (2014).

[44] N. Arakawa, Phys. Rev. B **91**, 159906(E) (2015).

[45] D. J. Luitz, *Numerical methods and applications to many fermion systems*, Ph.D. thesis, Universtät Würzburg (2013).

[46] M. Potthoff, Cond. Mat. Phys. **9**, 557 (2006).

[47] H. Hafermann, E. G. C. P. van Loon, M. I. Katsnelson, A. I. Lichtenstein, and O. Parcollet, Phys. Rev. B **90**, 235105 (2014).

[48] B. Kim, S. Khmelevskyi, I. I. Mazin, D. F. Agterberg, and C. Franchini, npj Quantum Mat. **2**, 37 (2017).

[49] This is a drastic suppression compared to RPA with bare interactions on the DMFT bubble with $T_{SDW} \sim 2500\,\mathrm{K}$ and the Hartree-Fock bubble with $T_{SDW} \sim 6850\,\mathrm{K}$.

[50] G.-Q. Liu, V. N. Antonov, O. Jepsen, and O. K. Andersen., Phys. Rev. Lett. **101**, 026408 (2008).

[51] Note that a similar observation has recently been made for the charge response of the cuprates [64].

[52] I. I. Mazin and D. J. Singh, Phys. Rev. Lett. **79**, 733 (1997).

[53] S. Hoshino and P. Werner, Phys. Rev. Lett. **115**, 247001 (2015).

[54] S. Hoshino and P. Werner, Phys. Rev. B **93**, 155161 (2016).

[55] K. Steiner, S. Hoshino, Y. Nomura, and P. Werner, Phys. Rev. B **94**, 075107 (2016).

[56] T.-H. Lee, A. Chubukov, H. Miao, and G. Kotliar, Phys. Rev. Lett. **121**, 187003 (2018).

[57] T. Vogt and D. J. Buttrey, Phys. Rev. B **52**, R9843 (1995).

[58] P. Blaha, K. Schwarz, G. K. H. Madsen, D. Kvasnicka, J. Luitz, R. Laskowski, F. Tran, and L. D. Marks, *WIEN2k, An Augmented Plane Wave + Local Orbitals Program for Calculating Crystal Properties* (Karlheinz Schwarz, Techn. Universität Wien, Austria, 2018).

[59] J. P. Perdew, K. Burke, and M. Ernzerhof, Phys. Rev. Lett. **77**, 3865 (1996).

[60] J. Kuneš, R. Arita, P. Wissgott, A. Toschi, H. Ikeda, and K. Held, Comput. Phys. Commun. **181**, 1888 (2010).

[61] N. Marzari and D. Vanderbilt, Phys. Rev. B **56**, 12847 (1997).

[62] A. A. Mostofi, J. R. Yates, Y.-S. Lee, I. Souza, D. Vanderbilt, and N. Marzari, Comput. Phys. Commun. **178**, 685 (2008).

[63] N. Marzari, A. A. Mostofi, J. R. Yates, I. Souza, and D. Vanderbilt, Rev. Mod. Phys. **84**, 1419 (2012).

[64] R. Nourafkan, M. Côté, and A.-M. S. Tremblay, Phys. Rev. B **99**, 035161 (2019).